Generalized hydrodynamics, normal-stress effects, and velocity slips in the cylindrical Couette flow of Lennard-Jones fluids

Roger E. Khayat and Byung Chan Eu*
Department of Chemistry, McGill University, 801 Sherbrooke Street West, Montreal, Quebec, Canada H3A 2K6
(Received 27 June 1988)

In this paper we extend the previous study of flow profiles in cylindrical Couette flow of a Lennard-Jones fluid so as to include the effects of normal stresses neglected in the previous work. The flow is subject to a temperature gradient and thermoviscous effects are taken into consideration. We apply the generalized hydrodynamic equations which are provided by the modified moment method for the Boltzmann equation reported previously. The results of calculation are in good agreement with the Monte Carlo direct simulation results of K. Nanbu [Phys. Fluids **27**, 2632 (1984)] and experimental data for all Knudsen numbers. The inclusion of normal stresses also brings about a new aspect to the flow properties which has not been seen before, since the flow profiles exhibit a phase-transition-like behavior as the Knudsen number increases beyond a critical value. There also appear slips in velocity at the inner cylinder wall in the supercritical regime of Knudsen number. At the critical Knudsen number the entropy production for the flow process also exhibits a singular behavior which is reminiscent of a second-order phase transition in thermodynamic systems.

I. INTRODUCTION

We have previously reported on the effects of nonlinear viscosity and heat conductivity on flow profiles of a Lennard-Jones fluid in plane[1] and cylindrical[2] Couette-flow geometry. The calculations of flow profiles were performed by using the generalized hydrodynamic equations which were derived from the Boltzmann equation by the modified moment method.[3] The generalized hydrodynamic equations fully conform to the requirements of the thermodynamic laws, and the fluid dynamics studies carried out were, in fact, applications of a theory[3,4] of extended irreversible thermodynamics developed by one of us. Since the principal aim of the calculations was exploratory and to show that the theory can yield some useful and practical results, the generalized hydrodynamic equations were limited to forms as simple as permitted by the problems in hand. Since the normal stresses are generally of second order in shear rate and thus appeared to be unimportant in their effect, they were neglected. Nevertheless, the density profiles thus calculated[2] were found to be in good agreement, for most of the Knudsen numbers studied, with the results by the Monte Carlo direct simulation method[5] and the classical Navier-Stokes equations with slip boundary conditions, but agreement with experiment[6] was only fair when the Knudsen number got large, as is also the case with the Monte Carlo direct simulation results. Therefore the results were encouraging, but indicated that the normal stresses neglected in the calculations might be important after all.

In this paper we report on a further study that takes normal stresses into consideration in the calculations of flow profiles in cylindrical Couette flow of a Lennard-Jones fluid. Inclusion of normal stresses not only improves the density profiles qualitatively in comparison with experiment, but also introduces new elements not encountered in gas dynamics before: they give rise to a phase-transition-like fluid behavior as the Knudsen number crosses a critical value, since the fluid behaves qualitatively differently beyond the critical point. For example, the gas that formerly did not exhibit a slip in velocity starts showing a noticeable slip as soon as the critical Knudsen number is exceeded. In fact, there is a qualitative change in all other fluid properties on transition of the fluid from the subcritical to the supercritical regime of Knudsen number. We believe that this aspect is new to fluid dynamics. It is also significant for the following reason. In gas dynamics slips[7] in velocity and temperature are often observed. Although they may be regarded as an approximation of boundary layers, they are commonly accounted for in terms of accommodation coefficients which appear in the slip boundary conditions[7] necessary for solving the Navier-Stokes and Fourier equations. In the Navier-Stokes–Fourier theory the viscosity and heat conductivity of the gas do not depend on density and therefore do not vanish with the density as they should. This defect gives rise to the inability of the Navier-Stokes flow profiles to exhibit a slip, or a thin boundary layer, which appears in the low-density regime, but the defect is repaired with modification of the boundary conditions, which is achieved by invoking diffuse and specular scattering off the wall by the molecules. In the present theory a velocity slip is brought about by nonlinear transport coefficients or shear and normal stresses which diminish in magnitude as the gas density decreases. In this regard we note that the boundary conditions used in this work are stick (no slip) boundary conditions as were used in the previous work.[2] Therefore the origin of the velocity slip in the present work is purely hydrodynamical, but not in the surface–gas molecule interaction. The mathematical mechanism for the slip and the phase-transition-like behavior will be discussed at an

appropriate stage. This phase-transition-like behavior appears more credible when we calculate the accompanying entropy production which is continuous but singular with respect to the Knudsen number in a manner similar to the behavior characteristic of a second-order phase transition. We find it rather intriguing, but its potential significance for fluid dynamics is not as yet fully understood.

In Sec. II the generalized hydrodynamic equations are presented. Since they appear in the previous papers[1,2] mentioned, only the essential equations will be presented in order to define the symbols and equations necessary for presenting the theory. In the same section the boundary conditions will be discussed for both subcritical and supercritical regions of Knudsen number. In Sec. III we present various numerical results which include flow profiles and shear stress, normal stresses and heat fluxes at the inner wall as a function of Knudsen number. They all exhibit a singular behavior. We also discuss the entropy production for the process which shows a singular behavior with respect to the Knudsen number. Section IV is for discussion and conclusion.

II. GENERALIZED HYDRODYNAMIC EQUATIONS

A. General forms of evolution equations

The modified moment method[3] of solution for the Boltzmann and generalized Boltzmann equation provides a set of generalized hydrodynamic equations within the framework of 13 moments:

$$\frac{\partial}{\partial t}\rho(\mathbf{r},t)=-\nabla\cdot\rho\mathbf{u}(\mathbf{r},t)\ , \tag{2.1}$$

$$\rho\frac{d}{dt}\mathbf{u}(\mathbf{r},t)=-\nabla\cdot\vec{\mathbf{P}}(\mathbf{r},t)\ , \tag{2.2}$$

$$\rho\frac{d}{dt}\mathcal{E}(\mathbf{r},t)=-\nabla\cdot\mathbf{Q}(\mathbf{r},\mathbf{t})-(\vec{\mathbf{P}}:\nabla\mathbf{u})\ , \tag{2.3}$$

$$\rho\frac{d}{dt}\underline{\hat{\mathbf{P}}}(\mathbf{r},t)=2p[\vec{\gamma}]^{(2)}+2\rho[\underline{\hat{\mathbf{P}}}\cdot\gamma]^{(2)}-\rho[\vec{\omega},\underline{\hat{\mathbf{P}}}]-\frac{p\rho\underline{\hat{\mathbf{P}}}}{\eta_0}(\sinh\kappa/\kappa)\ , \tag{2.4}$$

$$\rho\frac{d}{dt}\underline{\hat{\mathbf{Q}}}(\mathbf{r},t)=(\nabla\cdot\vec{\mathbf{P}})\cdot\underline{\hat{\mathbf{P}}}+\mathbf{Q}\cdot\vec{\gamma}-\hat{C}_p\vec{\mathbf{P}}\cdot\nabla T-\rho[\vec{\omega},\underline{\hat{\mathbf{Q}}}]-\frac{T\hat{C}_p p\rho\underline{\hat{\mathbf{Q}}}}{\lambda_0}(\sinh\kappa/\kappa)\ , \tag{2.5}$$

$$\rho\frac{d}{dt}\hat{\Delta}(\mathbf{r},t)=\tfrac{2}{3}\rho\underline{\hat{\mathbf{P}}}:\underline{\vec{\gamma}}-\tfrac{2}{3}\rho\hat{\Delta}\nabla\cdot\mathbf{u}-p\frac{d}{dt}\ln(pv^{5/3})-\frac{p(\rho\hat{\Delta}+p)}{\eta_{b0}}(\sinh\kappa/\kappa)\ , \tag{2.6}$$

where the flux evolution equations are in the Jaumann derivative form.[8,9] The symbols in (2.1)–(2.6) are defined as follows: $d/dt=(\partial/\partial t)+\mathbf{u}\cdot\nabla$, ρ is the mass density ($v=1/\rho$, specific volume), $\mathbf{u}$ is the fluid velocity, $\mathcal{E}$ is the internal energy, $\hat{C}_p$ is the specific-heat density at constant pressure, $\vec{\mathbf{P}}$ is the stress tensor, $\mathbf{Q}$ is the heat flux, p is the hydrostatic pressure, η_0 is the Newtonian (Chapman-Enskog) viscosity, λ_0 is the Fourier (Chapman-Enskog) thermal conductivity, η_{b0} is the bulk viscosity, m_r is the reduced mass, n is the number density, k_B is the Boltzmann constant, $\vec{\mathbf{U}}$ is the unit second-rank tensor, and

$$\vec{\gamma}=-\tfrac{1}{2}[\nabla\mathbf{u}+(\nabla\mathbf{u})^t]+\tfrac{1}{3}\vec{\mathbf{U}}\,\mathrm{tr}\vec{\mathbf{P}}\ ,$$

$$\vec{\omega}=\tfrac{1}{2}[\nabla\mathbf{u}-(\nabla\mathbf{u})^t]\ ,$$

$$\underline{\hat{\mathbf{P}}}=[\tfrac{1}{2}(\vec{\mathbf{P}}+\vec{\mathbf{P}}^t)-\tfrac{1}{3}\vec{\mathbf{U}}\,\mathrm{tr}\vec{\mathbf{P}}]/\rho\ ,$$

$$\hat{\Delta}=(\tfrac{1}{3}\,\mathrm{tr}\vec{\mathbf{P}}-p)/\rho\ ,$$

$$\underline{\hat{\mathbf{Q}}}=\mathbf{Q}/\rho\ ,$$

$$[\vec{\omega},A]=\vec{\omega}\cdot A-A\cdot\vec{\omega}\ ,$$

$$\kappa=\rho[(\tau_p/2\eta_0)^2\underline{\hat{\mathbf{P}}}:\underline{\hat{\mathbf{P}}}+(\tau_b/\eta_{b0})^2\hat{\Delta}^2+(\tau_q/\lambda_0)^2\underline{\hat{\mathbf{Q}}}\cdot\underline{\hat{\mathbf{Q}}}]^{1/2}\ ,$$

$$\tau_p=[2\eta_0(m_r k_B T/2)^{1/2}]^{1/2}/nk_B T\sigma\ ,$$

$$\tau_b=[\eta_{b0}(m_r k_B T/2)^{1/2}]^{1/2}/nk_B T\sigma\ ,$$

$$\tau_q=[\lambda_0(m_r k_B T/2)^{1/2}]^{1/2}/nk_B T\sigma\ .$$

The first three equations (2.1)–(2.3) are mass-, momentum-, and energy-conservation equations and the last three equations are the evolution equations for the traceless part $\rho\underline{\hat{\mathbf{P}}}$ and the excess trace $\rho\hat{\Delta}$ of the stress tensor $\vec{\mathbf{P}}$ and for the heat flux $\mathbf{Q}$. These evolution equations are the constitutive equations for the substance of interest. We have cast them in the Jaumann derivative form which is required of constitutive equations corotational with the frame of reference. The difference between the corotational and fixed frame constitutive equations is in the sign of the rotational terms $\rho[\vec{\omega},\underline{\hat{\mathbf{P}}}]$ and $\rho[\vec{\omega},\underline{\hat{\mathbf{Q}}}]$ which take on a negative sign[9] in the case of the corotational formulation. This sign change has an important significance since otherwise the constitutive equations do not behave correctly as have been pointed out previously.[2] The kinetic equations[3] such as the Boltzmann equation for dilute gases and the generalized Boltzmann equation for dense fluids yield constitutive equations containing higher-order moments, but the latter are neglected in (2.4)–(2.6) since the number of moments is limited to 13 in the present theory. The significance of the hyperbolic sine function in (2.4)–(2.6) is discussed in the previous papers[1,2] in this series to which the reader is referred for the details of it. It is related to the entropy production within the system and the latter will be later calculated for the system in hand. In the case of a fluid with no bulk viscosity we may set $\hat{\Delta}=0$. It is then necessary to consider only (2.4) and (2.5) for the constitutive equations for the system since it is possible to replace (2.6) with the gas equation of state especially for steady-state problems. Since we are considering such a case the set of generalized hydrodynamic equations consists of (2.1)–(2.5) in the present study. Since in the present work we are interested in the steady-state problem, we will set the time derivatives of the macroscopic variables in (2.1)–(2.5) equal to zero.

The system of interest here is a Lennard-Jones fluid

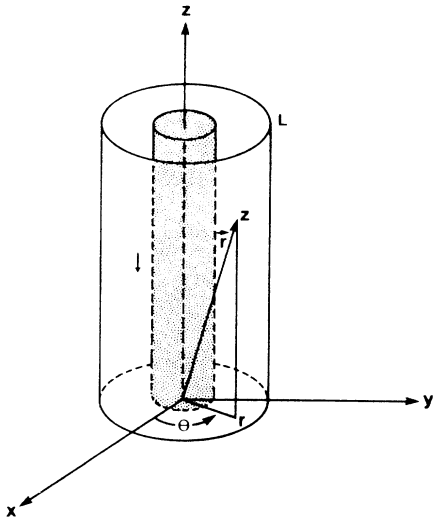

FIG. 1. Coordinates in the cylindrical Couette-flow geometry.

contained between two infinite concentric cylinders with radius R_i and R_o, respectively; see Fig. 1. The temperatures of the inner and outer cylinders are, respectively, T_i and T_o. The inner cylinder rotates at an angular velocity Ω while the outer cylinder is at rest. In some experiments the outer cylinder is also made to rotate in the opposite direction, but it does not basically change the analysis. The most convenient coordinates for the geometry of the system in hand are the cylindrical coordinates.

B. Steady-evolution equations in cylindrical coordinates

The macroscopic variables are then generally functions of r, θ, and z. We write various macroscopic variables in components:

$$\rho=\rho(r,\theta,z) ,$$

$$\mathcal{E}=\mathcal{E}(r,\theta,z) ,$$

$$\mathbf{u}=u_r(r,\theta,z)\delta_r+u_\theta(r,\theta,z)\delta_\theta+u_z(r,\theta,z)\delta_z ,$$

$$\rho\hat{\underline{P}}\equiv\vec{\vec{\Pi}}=\Pi_{rr}\delta_r\delta_r+\Pi_{r\theta}\delta_r\delta_\theta+\Pi_{rz}\delta_r\delta_r+\Pi_{\theta r}\delta_\theta\delta_r+\Pi_{\theta\theta}\delta_\theta\delta_\theta+\Pi_{\theta z}\delta_\theta\delta_z+\Pi_{zr}\delta_z\delta_r+\Pi_{z\theta}\delta_z\delta_\theta+\Pi_{zz}\delta_z\delta_z ,$$

$$\mathbf{Q}=Q_r(r,\theta,z)\delta_r+Q_\theta(r,\theta,z)\delta_\theta+Q_z(r,\theta,z)\delta_z ,$$

where δ_r, δ_θ, and δ_z are the orthogonal unit vectors in the cylindrical coordinate system, and the tensor components Π_{rr}, etc. are functions of r, θ, and z.

Because of the assumption of infinite cylinders, there is a translational symmetry along the z axis. Consequently, the fluid properties are translationally invariant in z and the macroscopic variables would not depend on z. Since there is also rotational symmetry with respect to the azimuthal angle θ, they are also independent of θ as well. In other words, the macroscopic variables are functions of r only. Taking the symmetry properties into account, we find the steady-state equations for (2.1)–(2.5) in cylindrical coordinates as follows:

$$\frac{d}{dr}(r\rho u_r)=0 , \tag{2.7}$$

$$\rho\left[u_r\frac{du_r}{dr}-\frac{u_\theta^2}{r}\right]=-\frac{d}{dr}(p+\Pi_{rr})-\frac{\Pi_{rr}-\Pi_{\theta\theta}}{r} , \tag{2.8a}$$

$$\rho\left[u_r\frac{du_\theta}{dr}+\frac{u_ru_\theta}{r}\right]=-\frac{1}{r^2}\frac{d}{dr}(r^2\Pi_{r\theta})+\frac{\Pi_{r\theta}-\Pi_{\theta r}}{r} , \tag{2.8b}$$

$$\rho u_r\frac{du_z}{dr}=-\frac{1}{r}\frac{d}{dr}(r\Pi_{rz}) , \tag{2.8c}$$

$$\rho u_r\frac{d\mathcal{E}}{dr}=-\frac{1}{r}\frac{d}{dr}rQ_r-\Pi_{\theta r}\frac{du_\theta}{dr}-\Pi_{zr}\frac{du_z}{dr}+\frac{\Pi_{r\theta}u_\theta-(p+\Pi_{\theta\theta})u_r}{r} , \tag{2.9}$$

$$\frac{p\Pi_{rr}}{\eta_0}q_e=-(\tfrac{8}{3}\gamma\Pi_{r\theta}+\tfrac{4}{3}\beta\Pi_{\theta z}) , \tag{2.10a}$$

$$\frac{p\Pi_{r\theta}}{\eta_0}q_e=-2p\gamma-(2\gamma\Pi_{\theta\theta}+\beta\Pi_{\theta z}) , \tag{2.10b}$$

$$\frac{p\Pi_{\theta\theta}}{\eta_0}q_e=\tfrac{4}{3}\gamma\Pi_{r\theta}-\tfrac{4}{3}\beta\Pi_{zr} , \tag{2.10c}$$

$$\frac{p\Pi_{rz}}{\eta_0}q_e=-2\gamma\Pi_{\theta z}-2\beta\Pi_{zz}-2p\beta , \tag{2.10d}$$

$$\frac{p\Pi_{\theta z}}{\eta_0}q_e=0 , \tag{2.10e}$$

$$\frac{p\Pi_{zz}}{\eta_0}q_e=\tfrac{4}{3}\gamma\Pi_{r\theta}+\tfrac{4}{3}\beta\Pi_{zr} , \tag{2.10f}$$

$$Q_rq_e=-\lambda_0\chi-(\lambda_0/\alpha)\left[(2\gamma+\omega)Q_\theta+\left[T\hat{C}_p\chi-\frac{u_\theta^2}{r}\right]\Pi_{rr}+3\beta Q_z\right] , \tag{2.11a}$$

$$Q_\theta q_e=-(\lambda_0/\alpha)\left[T\hat{C}_p\chi-\frac{u_\theta^2}{r}\right]\Pi_{\theta r}+(\lambda_0/\alpha)\omega Q_r , \tag{2.11b}$$

$$Q_zq_e=-(\lambda_0/\alpha)\left[T\hat{C}_p\chi-\frac{u_\theta^2}{r}\right]\Pi_{rz}-(\lambda_0/\alpha)(Q_r-2Q_z)\beta , \tag{2.11c}$$

where

$$\beta=\frac{1}{2}\frac{du_z}{dr} ,$$
$$\gamma=\frac{r}{2}\frac{d}{dr}(u_\theta/r) ,$$
$$\omega=(2r)^{-1}\frac{d}{dr}(ru_\theta) ,$$
$$\chi=\frac{d}{dr}\ln T , \tag{2.12}$$
$$\alpha=T\hat{C}_p p ,$$
$$q_e=\sinh\kappa/\kappa .$$

The symbol γ represents the shear rate and ω the rotation frequency. It is useful to note the following identity:

$$\omega-\frac{u_\theta}{r}=\gamma ,$$

so that, for example,

$$\tfrac{1}{3}\gamma+\omega-\frac{u_\theta}{r}=\tfrac{4}{3}\gamma ,$$
$$\tfrac{1}{3}\gamma-\omega+\frac{u_\theta}{r}=-\tfrac{2}{3}\gamma ,$$

etc. These identities appear in the evolution equations for Π_{rr}, etc. and Q_r, etc. The reader is referred to Ref. 2 for discussion on the relation of the Jaumann derivative to the presence of terms involving ω in the stress evolution equations (2.10a)–(2.10f).

Equation (2.7) integrates trivially to give

$$r\rho u_r=\text{const} . \tag{2.13}$$

Since $u_r=0$ at the boundaries, the integration constant must be equal to zero and we conclude

$$u_r=0 \text{ everywhere} . \tag{2.14}$$

This makes all the terms containing u_r in the set (2.7)–(2.12) vanish. This condition and the fact that $u_z=0$ at the boundaries can be used to show that

$$u_z=0, \text{ and } du_z/dr=0 \text{ everywhere} . \tag{2.15}$$

That is, $\beta=0$ everywhere. From (2.15), (2.11c), and (2.10e) follows the conclusion

$$\Pi_{z\theta}=\Pi_{\theta z}=\Pi_{rz}=\Pi_{zr}=0, \quad Q_z=0 . \tag{2.16}$$

It is also convenient to define the normal-stress differences N_1 and N_2 as follows:

$$N_1=\Pi_{\theta\theta}-\Pi_{rr} ,$$
$$N_2=\Pi_{rr}-\Pi_{zz} . \tag{2.17}$$

We will work in terms of normal-stress differences instead of the normal stresses themselves.

C. Reduced hydrodynamic equations

It is useful to cast the equations in reduced form by introducing suitable reduced variables. We therefore define the following reduced variables scaled by a suitably chosen set of reference variables. With the definitions

$$\Delta T=T_o-T_i ,$$
$$D=R_o-R_i ,$$

and denoting the reference set of variables by T_r, p_r, ρ_r, U_r, η_r, and λ_r for temperature, pressure, mass density, velocity, viscosity, and heat conductivity, respectively, we define the reduced variables

$$T^*=T/T_r ,$$
$$p^*=p/p_r ,$$
$$u^*=u_\theta/U_r ,$$
$$\rho^*=\rho/\rho_r ,$$
$$\xi=r/D ,$$
$$h^*=T\hat{C}_p/T_r\hat{C}_p(T_r) ,$$
$$\alpha^*=pT\hat{C}_p/p_rT_r\hat{C}_p(T_r) ,$$
$$\eta_0^*=\eta_0/\eta_r ,$$
$$\lambda_0^*=\lambda_0/\lambda_r ,$$
$$\gamma^*=\gamma/(U_r/D) ,$$
$$\chi^*=\chi D ,$$
$$\omega^*=\omega/(U_r/D) ,$$
$$\Pi^*=\Pi_{r\theta}/(\eta_r U_r/D) ,$$
$$Q^*=Q_r/(\lambda_r\Delta T/DT_r) ,$$
$$N_i^*=N_i/(\eta_r U_r/D) \quad (i=1,2) ,$$
$$Q_\theta^*=Q_\theta/(\lambda_r\Delta T/DT_r) .$$

Note that there is a factor of 2 difference between the reduced stress tensors in the present paper and those in Ref. 2. We find the present mode of reduction more appropriate. It, however, gives rise to a different numerical factor in some of the terms in the reduced equations appearing below. We will specify more explicitly the reference set of variables later when we perform numerical analysis. Since the dimensionless numbers above appear in a product form, we will find it convenient to define the following composite reduced numbers:

$$\delta\equiv(2\gamma_0/\pi)^{1/2}MK_n ,$$
$$\epsilon\equiv\Delta T/4T_rEP_r ,$$

where various nondimensional parameters are

$$M = U_r/(\gamma_0 R T_r)^{1/2}$$
$$(\gamma_0 = \hat{C}_p/\hat{C}_v,\quad R = \text{gas constant per unit mass}),$$
$$R_e = \rho_r U_r D/\eta_r ,$$
$$E = U_r^2/\hat{C}_p \Delta T \quad [\hat{C}_p = \hat{C}_p(T_r)] ,$$
$$P_r = \hat{C}_p \eta_r T_r/\lambda_r ,$$
$$K_n = l/D \quad (l = \text{mean free path}) .$$

Here M is the Mach number, R_e is the Reynolds number, E is the Eckert number, P_r is the Prandtl number, and K_n is the Knudsen number. Note that the Reynolds number is related to the Mach and Knudsen number as follows:

$$R_e = (\pi\gamma_0/2)^{1/2} M/K_n .$$

This means that the parameter δ may be expressed as

$$\delta = (2/\pi) R_e K_n^2 .$$

This mode of expression for δ provides another fluid dynamic aspect to the parameter. That is, since δ is a measure of importance of nonlinear transport processes, the latter will become important to flow properties as the value of R_e increases.

By collecting the various results above and using the reduced variables defined, we finally obtain the reduced generalized hydrodynamic equations:

$$\gamma_0 M^2 \frac{\rho^* u^{*2}}{\xi} = \frac{d}{d\xi}[p^* + \tfrac{1}{3}\delta(N_2^* - N_1^*)] - \delta N_1^*/\xi , \tag{2.18a}$$

$$\frac{d}{d\xi}(\xi^2 \Pi^*) = 0 , \tag{2.18b}$$

$$\frac{1}{\xi}\frac{d}{d\xi}(\xi Q^*) + 2P_r E \gamma^* \Pi^* = 0 , \tag{2.19}$$

$$\Pi^* q_e = -2\eta_0^* \gamma^* - \tfrac{2}{3}\delta(\eta_0^* \gamma^*/p^*)(2N_1^* + N_2^*) , \tag{2.20a}$$

$$N_1^* q_e = 4\delta(\eta_0^* \gamma^*/p^*)\Pi^* , \tag{2.20b}$$

$$N_2^* q_e = -4\delta(\eta_0^* \gamma^*/p^*)\Pi^* , \tag{2.20c}$$

$$Q^* q_e = -\lambda_0^* \chi^* - (\delta/P_r)(\lambda_0^*/\alpha^*)\left[(2\gamma^* + \omega^*) Q_\theta^* + \tfrac{2}{3} P_r \left(h^* \chi^* - E\frac{u^{*2}}{\xi} \right) \times (N_2^* - N_1^*) \right] , \tag{2.21a}$$

$$Q_\theta^* q_e = -(\delta/P_r)(\lambda_0^*/\alpha^*)\left[P_r \left(h^* \chi^* - E\frac{u^{*2}}{\xi} \right) \Pi^* - \omega^* Q^* \right] , \tag{2.21b}$$

where

$$q_e = \sinh\kappa/\kappa ,$$

with

$$\kappa = \delta\kappa^* ,$$
$$\kappa^* = (\pi^{3/2}\gamma_0)^{1/2}(T^{*1/4}/2\eta_0^{*1/2}p^*) \times [\Pi^{*2} + \tfrac{1}{3}(N_1^{*2} + N_2^{*2} + N_1^* N_2^*) + 4\epsilon(\eta_0^*/\lambda_0^*)(Q^{*2} + Q_\theta^{*2})]^{1/2} .$$

The parameter δ tends to zero as the fluid density increases since in that case K_n tends to zero.

Equations (2.18)–(2.21) are the generalized hydrodynamic equations which govern the cylindrical Couette flow in hand. We will solve them numerically. In Ref. 2 we have neglected the terms involving the parameter δ, that is, the following set is taken:

$$\gamma_0 M^2 \frac{\rho^* u^{*2}}{\xi} = \frac{dp^*}{d\xi} , \tag{2.22a}$$

$$\frac{d}{d\xi}(\xi^2 \Pi^*) = 0 , \tag{2.22b}$$

$$\frac{1}{\xi}\frac{d}{d\xi}(\xi Q^*) + 2P_r E \gamma^* \Pi^* = 0 , \tag{2.23}$$

$$\Pi^* q_e = -2\eta_0^* \gamma^* , \tag{2.24}$$

$$Q^* q_e = -\lambda_0^* \chi^* , \tag{2.25}$$

$$N_1^* = N_2^* = Q_\theta^* = 0 , \tag{2.26}$$

with

$$q_e = \sinh\kappa/\kappa \quad (\kappa = \delta\kappa^*) ,$$
$$\kappa^* = (\pi^{3/2}/\gamma_0)^{1/2}(T^{*1/4}/2\eta_0^{*1/2}p^*) \times [\Pi^{*2} + 4\epsilon(\eta_0^*/\lambda_0^*)Q^{*2}]^{1/2} . \tag{2.27}$$

The constitutive equations (2.24) and (2.25) are then simply the non-Newtonian stress equation and the non-Fourier heat flux equation which we have used in the previous studies.[1,2,10] These equations yield flow profiles comparable with the Monte Carlo simulation results by Nanbu[5] for all Knudsen numbers, but the results exhibit discrepancy with experiment in the high-Knudsen-number regime. In order to locate the source of the discrepancy, we carry out numerical analysis of a more complete set of generalized hydrodynamic equations, that is, (2.18)–(2.21), in this paper. If q_e is put equal to unity in (2.24) and (2.25), then the set of equations (2.22)–(2.25) becomes the Navier-Stokes and Fourier equations in the conventional hydrodynamics. Thus we clearly see the relation of the classical hydrodynamics to the present generalized hydrodynamics.

Let us now return to the generalized hydrodynamic equations (2.18)–(2.21). We observe that

$$N_1^* = -N_2^* . \tag{2.28}$$

Therefore N_2^* can be eliminated in (2.18) and (2.21), and the equation for N_2^*, (2.20c), drops out of the set. Besides the relation (2.28), there is another relation between the remaining stress tensor components Π^* and N_1^*. By eliminating q_e and $\eta^*\gamma^*$ from (2.20a) and (2.20b), we find

$$(N_1^* + 3p^*/2\delta)^2 + 6\Pi^{*2} = 9p^{*2}/4\delta^2 , \tag{2.29}$$

which is an ellipse in (Π^*, N_1^*) space. This stress ellipse is, in fact, the generator of a cone in the three-dimensional space (Π^*, N_1^*, p^*), and the solutions of the generalized hydrodynamic equations (2.18)–(2.21) are confined to a sector of the surface of the cone; see Fig. 2. It is convenient for the computational work performed in Sec. III if we introduce a new pressure defined by

$$p_r^* = p^*/\delta - 2N_1^*/3 \ .$$

We remark that this new variable is in fact the total normal stress divided by δ since $\Pi_{rr}^* = -2N_1^*/3$. This change of variable puts the stress ellipse in the form

$$(N_1^* + p_r^*/2)^2 + 2\Pi^* = \tfrac{1}{4} p_r^{*2} \ . \tag{2.29'}$$

The allowed sector of the surface is the part where

$$N_1^* = -\tfrac{1}{2} p_r^* \{1 - [1 - (8\Pi^{*2}/p_r^{*2})]^{1/2}\} \le 0 \ . \tag{2.30}$$

The branch of negative sign [i.e., the case where the square root in (2.30) is positive] leads to a solution of nonphysical behavior for N_1^*. Therefore the solutions of the generalized hydrodynamic equations are confined to the + half of the cone surface in Fig. 2. Since the normal-stress difference N_1^* must be real, the discriminant Δ in (2.30) must be positive semidefinite everywhere in ξ:

$$\Delta(\xi) = p_r^{*2} - 8\Pi^{*2} \ge 0 \ . \tag{2.31}$$

This inequality has an important significance in the present theory for the following reason.

We first indicate the significance of the recasting of the stress ellipse in the form of (2.29'). Since we find from (2.29)

$$p^* = -\delta(6\Pi^{*2} + N_1^{*2})/3N_1^* \ ,$$

we may cast (2.18a) into the form

$$dN_1^*/d\xi = -[N_1^*(R_e \rho^* u^{*2} + N_1^*) + 16\Pi^{*2}/3]/\xi(4N_1^*/3 + p^*/\delta) \ .$$

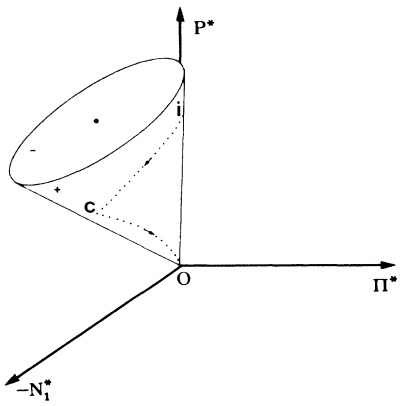

FIG. 2. Stress-pressure cone in (Π^*, N_1^*, p^*) space. The dotted curve shows a schematic trajectory followed by the solutions of the generalized hydrodynamic; note that the curve has a kink.

This equation is singular if the discriminant vanishes, since it is easy to show that

$$\Delta = p_r^{*2} - 8\Pi^{*2} = (4N_1^*/3 + p^*/\delta)^2 \ .$$

The discriminant indeed vanishes at the inner boundary for $K_n \ge K_n^c$ as we will see later.

As the density of gas decreases, the pressure obviously decreases and along with it also does the shear stress. This phenomenon also holds at the boundaries. As the gas density diminishes or the Knudsen number increases, the discriminant Δ rapidly decreases and eventually there is a point reached at which

$$\Delta(\xi_i) = 0 \quad (\xi_i = \xi \ \text{ at } r = R_i) \ . \tag{2.32}$$

See Fig. 3. In this connection we remark that it is numerically found

$$\Delta(\xi_i) > \Delta(\xi) \quad \text{for } \xi > \xi_i \ .$$

This is easily seen from the fact that p is lowest and Π^* is highest at $\xi = \xi_i$. The vanishing of the discriminant can be also understood in the following manner. The reduced generalized hydrodynamic equations (2.18)–(2.21) indicate that the normal stress will be comparatively negligible at low Knudsen numbers for which δ will be also small. As K_n or δ increases, N_1^* begins to be increasingly important in comparison with the shear stress and its magnitude increases since it is approximately proportional to δ at small δ; note that N_1^* is negative. However, Π^* decreases along with p_r^* as K_n increases. Since we obtain $-N_1^* = 2\Pi^{*2}/p_r^* + o(\Pi^{*4}/p_r^{*2})$, an increasing $-N_1^*$ means that the rates of decrease in Π^* and p_r^* are not the same, the latter being a little faster than the former. Thus there arises a point in K_n where Δ vanishes. The basic reason for a vanishing Δ is then seen to stem from the increasing magnitude of N_1^* as δ increases from zero, and $-N_1^*$ eventually reaches a maximum value allowed by (2.29'). Once this point is reached, the normal-stress difference or the normal stress itself cannot follow the same evolutionary path within the framework of the generalized hydrodynamic equations (2.18)–(2.21) with a given set of boundary conditions, but with another set

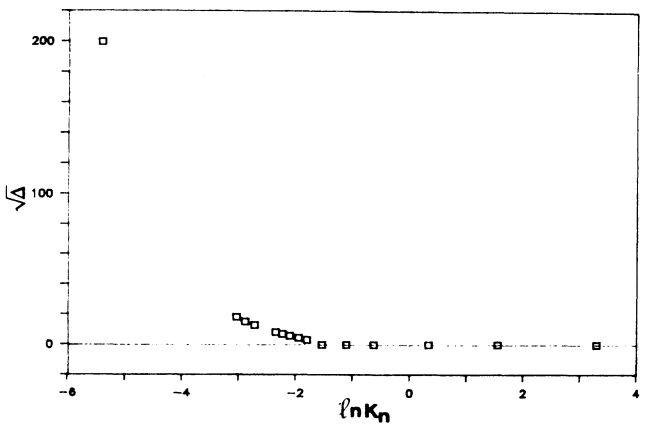

FIG. 3. Discriminant Δ vs $\ln K_n$.

modified by $\Delta=0$ as will be seen shortly.

Let us denote by K_n^c the Knudsen number at which Δ vanishes for the first time as K_n is increased from zero. We will call it the critical Knudsen number. Condition (2.32) must hold for all $K_n \geq K_n^c$, or there are no physical solutions for the generalized hydrodynamic equations subject to the boundary conditions imposed, because the solutions will turn out to be complex. Thus it is necessary to demand that $\Delta(\xi_i)=0$ for all $K_n \geq K_n^c$. Since this condition fixes the value of p_r^* at the inner boundary in terms of $\Pi^*(\xi_i)$, the system of equations (2.18)–(2.21) is presented with an additional boundary condition that arises since we require that the solutions be real for $K_n \geq K_n^c$. This appearance of a boundary condition for p_r^* (or pressure indirectly) frees a boundary condition on velocity or temperature. We choose the boundary condition on the tangential velocity at the inner wall as the one to be eliminated in favor of the pressure boundary condition newly created by $\Delta(\xi_i)=0$. There are reasons to indicate that it is the logical one to eliminate. We will return to this question when we discuss the boundary conditions. This phenomenon of a vanishing discriminant has important consequences for flow profiles as we will show later. We remark that Lin and Street[11] in the theory applying the Navier-Stokes equation took the boundary condition on pressure to be the mean pressure in order to calculate flow profiles within the framework of the Burnett equations,[12] but there is no physical and experimental reason to support their choice. In the present theory with inclusion of normal stresses the pressure boundary condition appears as a condition for the solutions of generalized hydrodynamic equations to be real, and that condition is not the mean pressure of the gas.

D. Boundary conditions

The generalized hydrodynamic equations (2.18)–(2.21) require five boundary conditions. The specification of the velocity and temperature at the inner and outer cylinders takes care of four boundary conditions. The choice of the fifth condition is not obvious for the experimental condition of the present problem since neither the pressure nor the density of the fluid is measured at either one of the boundaries (i.e., cylinders). As in the previous work,[2] for the remaining boundary condition we take advantage of the fact that the mass of the fluid between the two cylinders is conserved in time. Therefore the initial (uniform) experimental density must be equal to the average steady-state density:

$$\rho_0=\langle\rho(r)\rangle\equiv[2\pi(R_o^2-R_i^2)]^{-1}2\pi\int_{R_i}^{R_o}dr\, r\rho(r)\ , \tag{2.33}$$

where ρ_0 is the initial uniform mass density and $\rho(r)$ is the steady-state mass density. Once the initial density ρ_0 is given, the density profile can be determined subject to (2.33) in a way consistent with all other boundary conditions. Equation (2.33) constitutes the desired fifth condition which makes the problem well posed. This will be cast in a reduced form later.

1. *Boundary conditions in the subcritical regime*

In the case of $K_n < K_n^c$ the gas behaves normally since the density is in the normal range and the boundary conditions are the usual stick boundary conditions in addition to (2.33). Therefore, for the velocities and temperatures at the boundaries, we impose the boundary conditions

$$\left.\begin{matrix} u^*=1 \\ T^*=T_i/T_r \end{matrix}\right\}\text{at } \xi=\xi_i \tag{2.34a}$$

and

$$\left.\begin{matrix} u^*=0 \\ T^*=T_o/T_r \end{matrix}\right\}\text{at } \xi=\xi_o\ , \tag{2.34b}$$

$$\langle\rho^*(\xi)\rangle=1\ , \tag{2.34c}$$

which we have put in reduced forms. These and those given below [i.e., (2.35a) and (2.35b)] are the stick boundary conditions which are traditionally considered applicable to gases at or above the normal density for which the Knudsen number is sufficiently small. It is a common practice in gas dynamics to take slip boundary conditions as the gas density diminishes. The proposition we make in this series of work is that the transport processes in low-density gases are basically nonlinear and slip phenomena observed in the laboratory are a manifestation and consequence of nonlinear transport processes; *it is sufficient to use the stick boundary conditions, provided the transport processes are appropriately nonlinear.* As in a previous work[2] this proposition withstands comparison with independent results by Nanbu[5] and with experiment. The present model includes normal stresses neglected in the previous work and thus is in further support of the proposition.

2. *Boundary conditions in the supercritical regime*

In the supercritical regime of $K_n \geq K_n^c$ the discriminant $\Delta(\xi_i)$ vanishes and this ensures real solutions. However, since it adds another boundary condition, the problem becomes overdetermined. This problem is easily overcome if one of the boundary conditions in (2.34a)–(2.34c) is eliminated. We choose the following boundary conditions:

$$\left.\begin{matrix} p_r^*=\sqrt{8}\Pi^*/\delta \\ T^*=T_i/T_r \end{matrix}\right\}\text{at } \xi=\xi_i\ , \tag{2.35a}$$

$$\left.\begin{matrix} u^*=0 \\ T^*=T_o/T_r \end{matrix}\right\}\text{at } \xi=\xi_o\ , \tag{2.35b}$$

$$\langle\rho^*(\xi)\rangle=1\ . \tag{2.35c}$$

We have replaced one of the velocity boundary conditions with the boundary condition on p_r^* at the inner wall on the basis of the following reasoning. The density condition cannot be replaced since it not only does not change the situation in which acceptable real solutions would not otherwise arise, but also it would be unlikely to be satisfied by the density profile even if the solutions were possible. The temperature boundary conditions do not seem to be sensible candidates because gas molecules should acquire the temperatures of the walls especially in

view of the fact that gas molecules interact with the particles forming the walls. After all, the gas molecules can even get adsorbed on the walls. Finally, it is quite sensible on the physical ground that nothing extraordinary is expected to occur at the outer wall and consequently the velocity of the gas should be equal to zero at the stationary outer wall. Thus the choice we have made for the boundary conditions above.

The p_r^* boundary condition, on substitution into (2.30), yields N_1^* at the boundary in the form

$$N_1^* = -\sqrt{2}\Pi^* ,$$

which implies $p^* = 4\sqrt{2}\Pi^*\delta/3$ at the inner boundary.

E. Linear transport coefficients η_0 and λ_0

There are two transport coefficients appearing in this theory that must be supplied before solutions are attempted. They are the zero shear rate shear viscosity and the zero temperature gradient heat conductivity. They can be calculated by means of the first-order Chapman-Enskog theory.[12] In this work we use the formulas proposed by Ashurst and Hoover[13(a)] for a Lennard-Jones fluid. They were used in our previous work.[1,2] A similar formula for viscosity was derived by one[13(b)] of the present authors from the kinetic theory based on the generalized Boltzmann equation. They are

$$\eta_0 = [0.171 + 0.0152[1 - 0.5(\bar{\epsilon}/k_B T)^{1/2} + 2\bar{\epsilon}/k_B T](\exp\{7.02[1 - 0.2(\bar{\epsilon}/k_B T)^{1/2}]\bar{x}\} - 1)](m\bar{\epsilon})^{1/2}\sigma^{-2}(k_B T/\bar{\epsilon})^{2/3} ,$$

$$\lambda_0 = \{0.642 + 0.36[\exp(3.76\bar{x}) - 1]\}\sigma^{-2}(\bar{\epsilon}/m)^{1/2}(k_B T/\bar{\epsilon})^{2/3} k_B T ,$$

where

$$\bar{x} = n\sigma^3(\bar{\epsilon}/k_B T)^{1/4} ,$$

$\bar{\epsilon}$ is the well depth of the interaction potential, m is the mass of the fluid molecules, and σ is the Lennard-Jones potential size parameter. At the normal density or below, the exponential factors are practically equal to unity and we have

$$\eta_0 = 0.171(m\bar{\epsilon})^{1/2}\sigma^{-2}(k_B T/\bar{\epsilon})^{2/3} ,$$

$$\lambda_0 = 0.642\sigma^{-2}(\bar{\epsilon}/m)^{1/2}(k_B T/\bar{\epsilon})^{2/3} k_B T .$$

III. SOLUTION OF THE GENERALIZED HYDRODYNAMIC EQUATIONS AND FLOW PROFILES

Since Alofs and Springer[6] reported on density profiles of argon in cylindrical Couette flow, we make comparison of our results with theirs. We take the initial density obtained from the reported chamber pressure and temperature in their experiment. The reference temperature is taken to correspond to the mean value of the wall temperatures. Other reference values are taken to correspond to the experimental condition. With these reference quantities, we determine various dimensionless parameters such as M, K_n, P_r, E, the aspect ratio, and the reference transport coefficients $[\eta_r = \eta_0(T_r, n_r)$, $\lambda_r = \lambda_0(T_r, n_r)]$.

The solution procedure for (2.18)–(2.21) is basically the same as the one we have used in Ref. 2. We first integrate (2.18a) and (2.18b) to obtain

$$\Pi^* = C_1\xi^{-2} ,$$

$$Q^* = 2P_r E(C_2\xi^{-1} - C_1 u^*\xi^{-2}) ,$$

where C_1 and C_2 are the integration constants. These results are substituted into the rest of the equations which are afterward solved subject to the boundary conditions (2.34a)–(2.34c) in the subcritical regime of Knudsen number and the boundary conditions (2.35a)–(2.35c) in the supercritical regime. As in the previous work, we use a combination of the shooting method and the sixth-order Runge-Kutta method for integration of the equations.

The values of C_1 and C_2 are first guessed together with a value of the pressure (or density) at one of the cylinder walls and the governing equations are solved in an attempt to satisfy the four boundary conditions and reach an average reduced density equal to unity. This procedure is repeated until an imposed tolerance is satisfied. Since this technique is rather tedious, we have devised a modified Newton-Raphson iterative scheme that would automatically determine the appropriate values of the two constants and pressure (or density) at the boundary.

In order to compare our results with those obtained experimentally we have to use the same values for the dimensionless parameters involved. There is, however, some ambiguity in the way some of the parameters were defined and in the choice of some reference quantities taken in the experiment. The wall temperatures were initially identical, but the wall temperatures at steady state, however, were found to be different by 8 °C. We therefore defined our Mach number on the basis of the mean value of the two steady-state wall temperatures. The mean value is then our reference temperature. The Mach number thus calculated turns out to be comparable to that used by Alofs and Springer, i.e., 0.9908 for ours compared to 0.9917 for theirs. This is the value for M we use throughout this work. The aspect ratio A, and the Eckert and Prandtl numbers are set equal to the experimental conditions, i.e., $A = \frac{2}{3}$, $E = 25.115$, and $P_r = 0.666$. Note that the specification of the Eckert number fixes that of the temperature ratio T_i/T_o. The Chapman-Enskog transport coefficients are those for a Lennard-Jones gas, while the ones used in the experiment[6] are based on the Maxwellian model for the intermolecular force. For this reason the K_n values in the present investigation are slightly higher than the values quoted in the paper by Alofs and Springer[6] and by Nanbu[5] although they are both based on the same value of the initial density.

Although the present calculations cover all flow prop-

erties, only the density profiles can be compared with the experimental results since others are experimentally unavailable. In the experiment by Alofs and Springer[6] the initial chamber pressures varied from 0.050 to 0.0020 mm Hg (i.e., 1.58×10^{-7} and 0.06×10^{-7} in the units of $\bar{\epsilon}/\sigma^3$) with corresponding Knudsen number ranging from 0.0426 to 1.065. When compared to the present choice of reference variables, the Knudsen numbers range from 0.0544 to 1.3962.

The density profiles for different initial chamber pressures are shown in Figs. 4 and 5, where the + symbols represent the experimental data,[6] the squares the simulation results by Nanbu,[5] and the solid curve the solutions by the present theory. They are of particular interest since density measurements were mainly the object of attention in the experiment.[6] In the figures we have left out the results computed by the Navier-Stokes theory with slip boundary conditions since they were compared with others in a previous work.[2] The critical Knudsen number is found to be $K_n^c=0.2257$. In the case of $K_n=0.0544$ and 0.1046 the results by the present theory agree with both the Monte Carlo simulation results and experiment, although for both the present and Monte Carlo results there are discernible discrepancies with experiment near the walls. These discrepancies get more noticeable in the case of $K_n=0.1388$ although the differences are within a few percent. In the subcritical range the density profiles calculated with[2] and without normal stresses are virtually identical.

As K_n passes the critical value, the density profiles by the present theory flatten more and approach the experimental data a little better than those calculated without normal stresses in the previous work,[2] but in the vicinity of the inner wall they also exhibit a pronounced boundary layer in the opposite sense to the profiles by the Monte Carlo direct simulation method[5] and in the previous work.[2] In the absence of more detailed experimental data in the vicinity of the walls which are very difficult to measure precisely owing to the interference by the walls , it is difficult at present to establish the true picture of the density profiles near the walls. However, it seems worthwhile to examine and compare profiles by the Monte Carlo method and the present theory.

As K_n increases, the Monte Carlo density profiles begin to show a minimum near the inner wall. In fact, Nanbu's calculation[5] shows that the pressure is larger

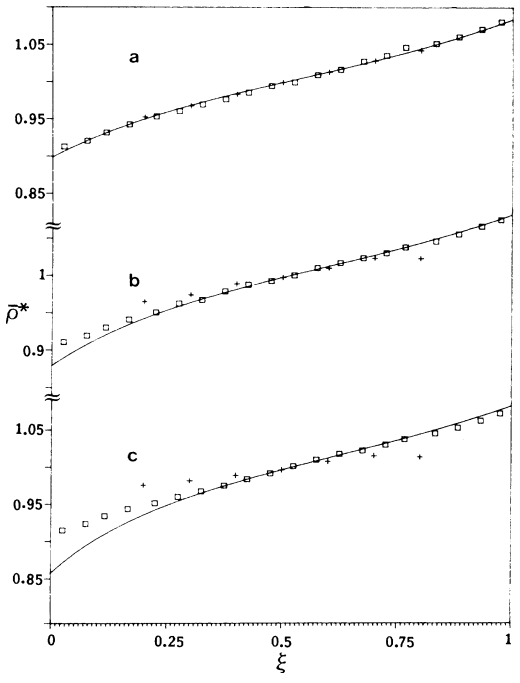

FIG. 4. Reduced density vs reduced distance. Curve *a*, $K_n=0.0544$ and $p_0=0.05$ mm Hg ($1.58\times10^{-7}\bar{\epsilon}/\sigma^3$; this unit will be referred to as the LJ unit henceforth). $\bar{\rho}^*=\rho/\rho_{\text{midstream}}$. When converted into $m\sigma^{-3}$, $\rho_m^*\equiv\rho_{\text{midstream}}$, $\sigma^3/m=0.62\times10^{-7}$. The same notation is used in the subsequent figures. +, experimental value of Alofs and Springer; □, Monte Carlo direct simulation value by Nanbu; ——, the present theory. Curve *b*, $K_n=0.1046$ and $p_0=0.026$ mm Hg (0.82×10^{-7} LJ units). $\rho_m^*=0.32\times10^{-7}$. Curve *c*, $K_n=0.1388$ and $p_0=0.001\,96$ mm Hg (0.62×10^{-7} LJ units).

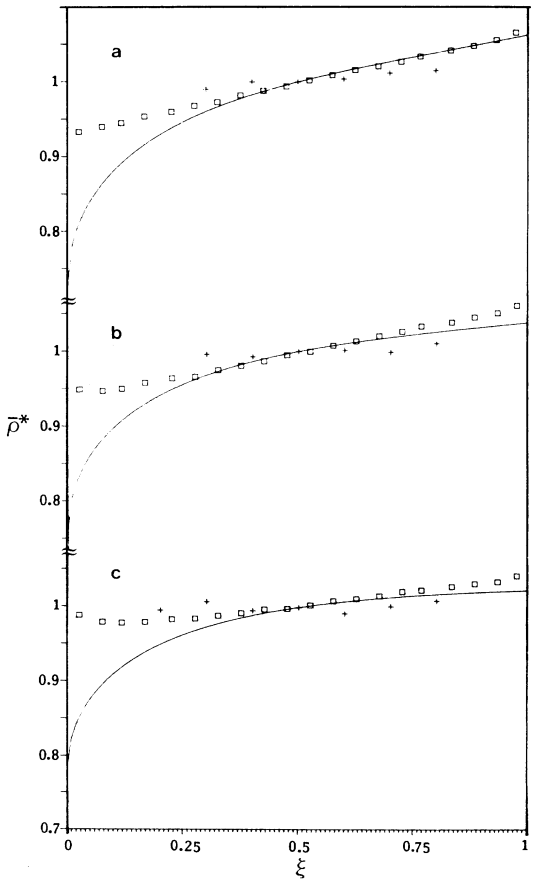

FIG. 5. Reduced density vs reduced distance. Curve *a*, $K_n=0.3201$ and $p_0=0.0085$ mm Hg (0.27×10^{-7} LJ units). +, experiment; □, simulation; ——, the present theory. $\rho_m^*=0.11\times10^{-7}$. Curve *b*, $K_n=0.5184$ and $p_0=0.005\,25$ mm Hg (0.17×10^{-7} LJ units). $\rho_m^*=0.066\times10^{-7}$. Curve *c*, $K_n=1.362$ and $p_0=0.009$ mm Hg (0.06×10^{-7} LJ units). $\rho_m^*=0.015\times10^{-7}$.

than its midstream values when the Knudsen number gets much larger, see Fig. 4 in Nanbu's paper. Such a minimum in density profiles appeared in our previous work[2] in which the normal stresses were neglected. Contrary to these results, the density profiles by the present theory do not show a minimum, but instead a boundary layer which gets increasingly thinner as K_n gets larger. A similar behavior is exhibited by the pressure (Fig. 9 below). In contrast to the pressure or the density, for K_n much larger than K_n^c the total normal force p_r^* (i.e., the total pressure) becomes larger near the inner wall than in the midstream value as is shown in Fig. 10 below. In fact, the behavior of p_r^* looks rather like that displayed by the pressure profiles in Nanbu's paper,[5] and we wonder if his pressure was not indeed the same as the total normal force p_r^* calculated here. Incidentally, this enhanced value of p_r^* near the inner wall seems to be in accord with the phenomenon observed by Reiner,[14(a)] who observed that a rotating disk above a gas can be suspended by the gas it is shearing. Normal stresses were believed to be the cause for the phenomenon although full confirmation of it is not available as yet. The result of the present calculation seems to support this viewpoint. Normal stresses are also important for flow properties of highly viscous liquids such as polymers and polymer solutions which display Weissenberg's effects.[14(b)] We then begin to wonder about the reason. For this we must recognize that the normal stresses become comparatively significant in both gases and liquids for basically the same reason that the parameter δ becomes large whether the fluid is a gas or a liquid. In the case of rarefied gas the parameter δ becomes large since K_n increases for the reason that the density decreases, while in the case of a liquid the "Knudsen number," which may be defined in terms of an effective range of momentum transfer in the liquid, becomes large because the momenta get transferred to a longer distance owing to a long-range correlation of particles and therefore the viscosity becomes large. (Note that the thermal conductivity increases with the viscosity.) Either way, the parameter δ becomes large and the normal stresses become as important as the shear stresses and the pressure. Therefore we might be able to say that rarefied gases and highly viscous liquids are similar as far as the importance of normal stresses is concerned.

In rarefied gas dynamics there is also a prevalent misconception regarding the relation between the Knudsen number and what is called free molecular flow. We consider it with the cylindrical Couette flow in hand. The Knudsen number in this case is defined in terms of the gap width D between the two cylinders while the length of the cylinder is assumed infinite or, at least, very long. Now, if the gas density is such that K_n so defined is larger than or near unity, we are told to imagine that molecules do not have much chance to collide with each other on their flights between the walls. This would be certainly true if all the molecules shuttled between the two walls in the perpendicular direction to the walls, but the probabilities of such collisions with the walls are rather small. More predominant kinds of collisions with the walls would be small-angle, slanted scatterings off the walls. Particles undergoing small-angle, slanted collisions with a wall would never lack a chance or more to collide with other particles on their flight to the other side of the cylinder wall, since the cylinders are infinitely long by assumption and the mean free path is finite if the density is low but finite. Therefore the gas behaves as a continuum in the axial, or near-axial, direction even if $K_n \gtrsim 1$. This consideration shows that the gas should be diluted much more than it is required for $K_n \approx 1$ before it exhibits a free molecular flow behavior in all directions. In rarefied gas dynamics[7] a kinetic equation without a collision term is often taken along with a suitable boundary condition on the distribution function on the basis of the free molecular flow argument mentioned above. It looks plausible at first glance, but as we have indicated above, there is a physical flaw in it and such an approximation should not be satisfactory for Knudsen numbers not so large.

From the generalized hydrodynamic equations presented, we see that the normal-stress effects and probably other nonlinear effects take over and significantly influence the flow behavior before a free molecular flow sets in. It appears that the boundary layers exhibited by the density profiles obtained by the present theory are a manifestation of such normal-stress and nonlinear effects. We have, in fact, found through monitoring numerical solutions and their position dependence that the normal stresses help the centrifugal (inertia) force push the fluid toward the outer wall, and this partly accounts for the density profiles calculated in this work.

From the consideration made above we are also able to infer that in the Monte Carlo direct simulation method the normal stresses may have been somehow neglected by the design of the algorithm or the approximation made to the kinetic equation, e.g., the decoupling approximation.[15]

In Fig. 6 are presented velocity profiles for various Knudsen numbers. The profiles 1, 2, and 3 are, respectively, for $K_n = 0.0544$, 0.1046, and 0.1388 which are subcritical, i.e., less than $K_n^c = 0.2257$, while the profiles 4, 5, and 6 are for supercritical values of K_n: 0.3201, 0.5184,

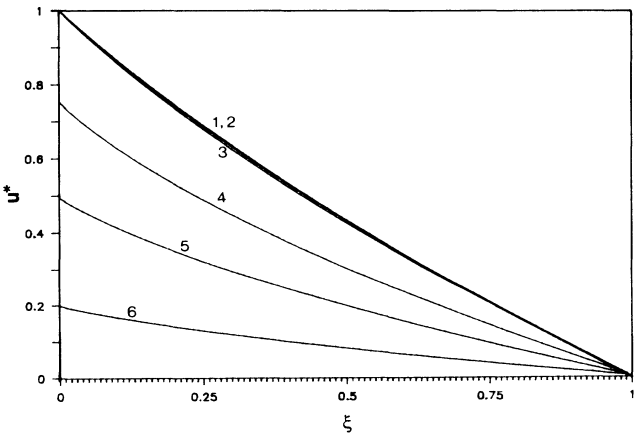

FIG. 6. Reduced velocity profiles for various values of K_n: Curve 1, 0.0544; curve 2, 0.1046; curve 3, 0.1388; curve 4, 0.3201; curve 5, 0.5184; curve 6, 1.362.

and 1.362, respectively. This manner of numbering profiles will be used in Figs. 8–13. The subcritical profiles are almost identical and linear, the slight curvings being due to the centrifugal effect. The supercritical profiles show a slip which increases with increasing K_n. The origin of the slips seen here is completely hydrodynamical, since they have nothing to do with surface–gas molecule interaction to which slips are commonly attributed[7] in rarefied gas dynamics. The slips are intimately tied up with the vanishing discriminant at $K_n \geq K_n^c$, which not only compels us to switch over from the subcritical to the supercritical boundary conditions, but also thereby makes all the fluid variables behave differently in the regions of $K_n > K_n^c$ and $K_n < K_n^c$; see Figs. 14–18 below. Since it is interesting to see the K_n dependence of velocity slip, in Fig. 7 we have plotted $\Delta u \equiv 1 - u^*$ versus $\ln K_n$, where u^* is the velocity at the inner wall. The slip starts at the critical Knudsen number and rises steeply, reaching unity eventually in the high-Knudsen-number regime. The behavior is reminiscent of a phase transition since a qualitatively different solution emerges as K_n crosses the critical value. In fact, the figure reminds us of the magnetization versus magnetic field curve in a Heisenberg magnet system undergoing a second-order phase transition. In Fig. 7 the crosses represent the values obtained from (2.18)–(2.21), and the squares are those obtained with q_e put equal to unity. In the latter case we have linear dissipation terms in the evolution equations in the set (2.18)–(2.21), which now correspond, except for the nonlinear terms in (2.20a)–(2.21b), to the corotational Maxwell equation[16] for the stress tensor and the Cattaneo-Vernotte equation[17] for the heat flux. The slip values show that the nonlinear dissipative terms have minor effects on velocity slips near the critical Knudsen number. This comparison indicates that slips are principally due to the normal stresses and would be a universal feature in all fluid flows as long as normal stresses are not neligigible. The Knudsen number dependence of the velocity slips calculated can be fitted to the following formula:

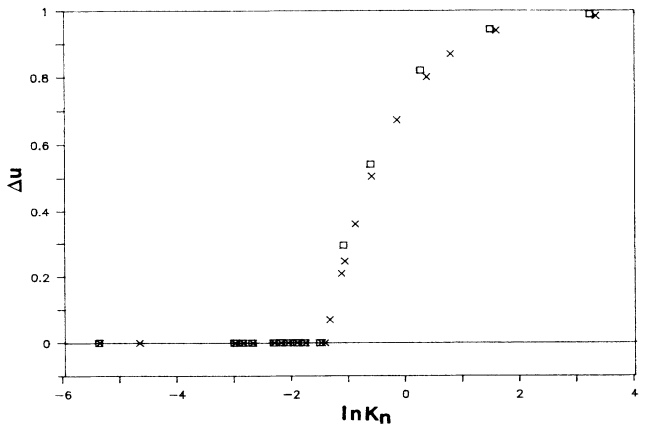

FIG. 7. Δu vs $\ln K_n$. ×, values for $q_e \neq 1$, i.e., solutions of (2.18)–(2.21); □, values for $q_e = 1$, i.e., for corotational Maxwell and Cattaneo-Vernotte slip below K_n^c.

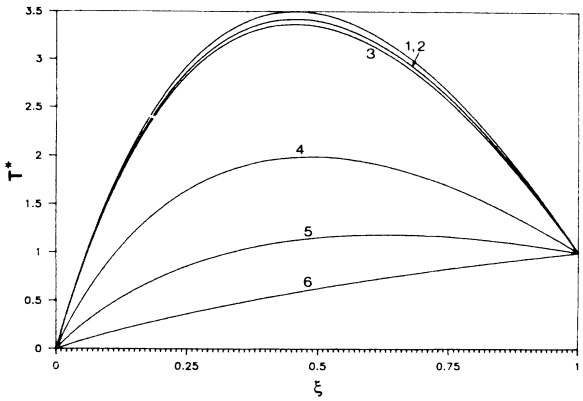

FIG. 8. Reduced temperature profiles for various values of K_n. The values of the Knudsen numbers are the same as in Fig. 10. In the units of $k_B/\bar{\epsilon}$ [i.e., temperature (reference temperature)] $T_r = (T_i + T_0)/2 = 2.563$ and $\Delta T = 0.0668$. Thus in the LJ units $T^*_{LJ} = 0.0668 T^* + 2.529$, where T^* is a temperature in the figure.

$$\Delta u \equiv 1 - u^* = 1.0167 - 0.0740 \sinh^{-1}[12.5(K_n - K_n^c)]/(K_n - K_n^c) , \tag{3.1}$$

where $K_n \geq K_n^c$. We mention that the effective viscosity (i.e., non-Newtonian viscosity[18]) approximately depends on the Knudsen number like an inverse hyperbolic sine function. Note that δ is proportional to K_n.

In Figs. 8–10 are plotted temperature, pressure, and total normal force (p_r^*) profiles for K_n ranging from 0.0544 to 1.3621. They are labeled 1–6; curves 1–3 are for the subcritical values of K_n as indicated in the previous figures, while curves 4–6 are for the supercritical values. The subcritical temperature profiles have thinner boundary layers than the supercritical profiles, and they are due to a larger viscous heating effect which is more effective at higher gas densities. The viscous heating effect practically disappears by the time $K_n = 1.3621$ is reached. We have already mentioned that the p_r^* profiles

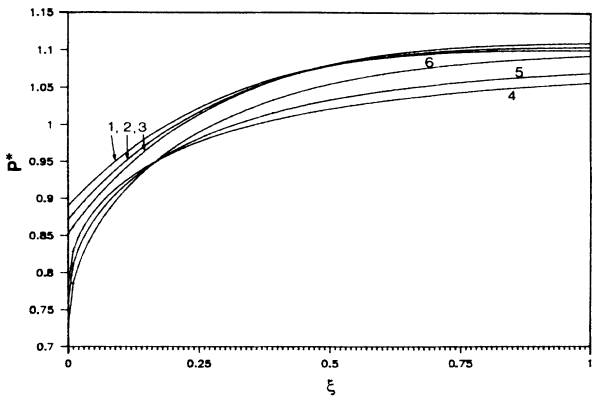

FIG. 9. Reduced pressure profiles for various values of K_n.

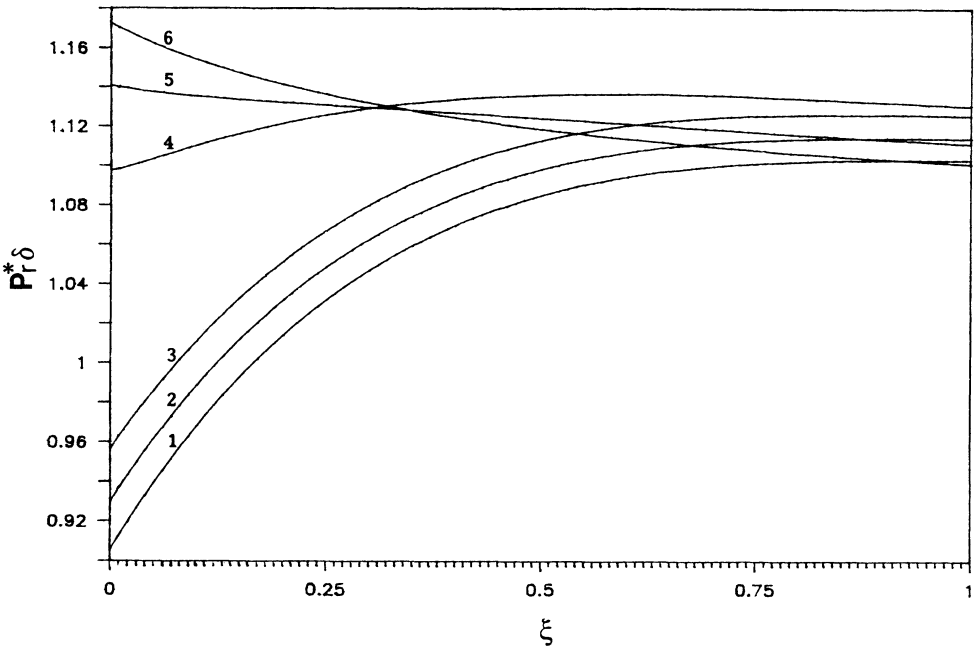

FIG. 10. Reduced total normal force profiles for various values of K_n. Notice that the inner wall values of $p_r^*\delta$ are larger than its values of the midstream or beyond. The behavior is reminiscent of Reiner's effect.

are reminiscent of the pressure profiles in Nanbu's Monte Carlo study,[5] since the enhanced profiles of p_r^* near the inner wall exhibited by curves 5 and 6 are exactly the same as those shown by his pressure profiles at the same Knudsen numbers. This behavior of p_r^* near the inner wall in the supercritical region of K_n is interesting since it means that the inner wall is exerted on by a total normal force larger than that in the midstream or beyond. It is thus suggestive of Reiner's effect.[14(a)]

We have calculated the profiles for the shear stress, normal stress, and radial and tangential heat fluxes. Except for the normal-stress difference, they decrease monotonically for all Knudsen numbers, while N_1^* increases monotonically toward zero from negative values for all K_n. The heat fluxes, however, behave somewhat differently and present a little more complicated pattern, since there is a changeover from one pattern to another as K_n crosses K_n^c. Although they are interesting, we do not present them here for lack of space. More interesting and perhaps more insightful quantities are the effective transport coefficients η^*, ψ_1^*, and λ^* which are defined by

$$\Pi^* = -\eta^*\gamma^* ,$$
$$N_1^* = -\psi_1^*\gamma^{*2} , \tag{3.2}$$
$$Q^* = -\lambda^*\chi^* + O(\chi^*\gamma^*) \simeq -(\lambda_0^*/q_e)\chi^* + O(\chi^*\gamma^*) ,$$

which we have plotted in Figs. 11–13. They distinctly depend on position. Therefore the notion of transport coefficients is not very useful if the transport processes of

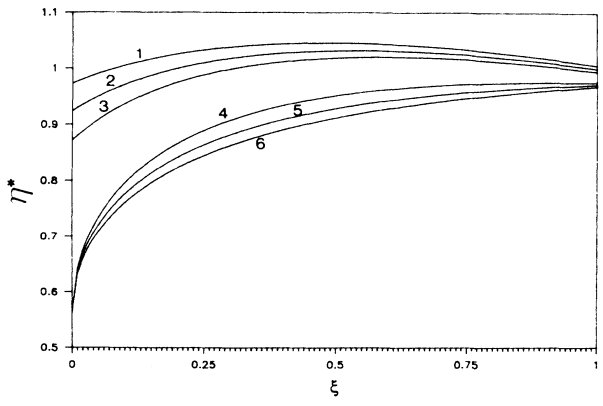

FIG. 11. Reduced viscosity profiles for various Knudsen numbers.

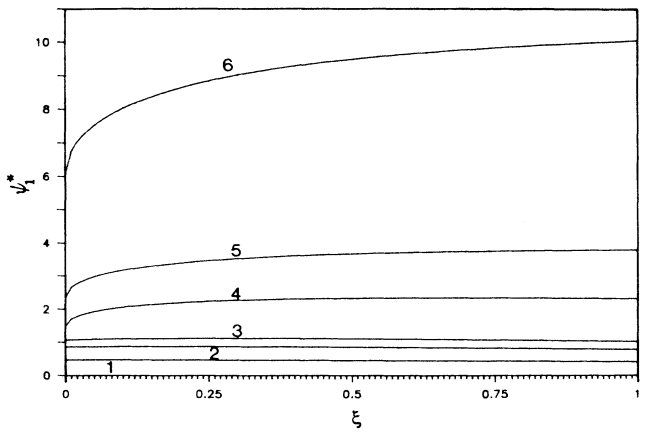

FIG. 12. Reduced primary normal-stress coefficient for various Knudsen numbers.

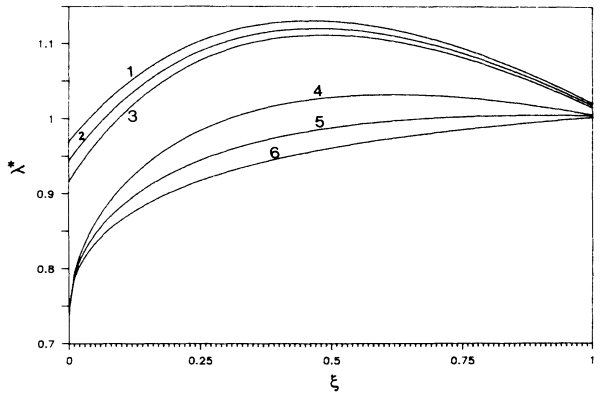

FIG. 13. Reduced thermal conductivity for various Knudsen numbers.

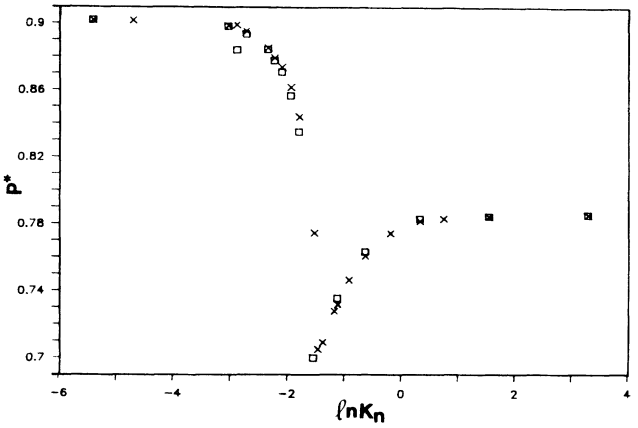

FIG. 15. Reduced pressure at the inner wall vs $\ln K_n$. The meanings of the symbols are the same as in Figs. 17 and 14.

interest are nonlinear, although they are routinely used in rheology and other fields that deal with nonlinear transport phenomena. We believe that they should be taken as a representation of constitutive relations of the substance in question, but unless they are given over the entire range of space, their utility appears to be rather limited according to the figures presented. In this connection we point out that viscosity and normal-stress coefficients are commonly measured on the basis of the narrow gap approximation[19] which ignores the effect of the position dependence of shear rate. A recent analytic calculation[20] of the effective viscosity for tube flow under pressure also supports the precautionary remark on the usefulness of effective transport coefficients.

In order to better understand the behavior of the microscopic variables in the subcritical and supercritical region of Knudsen number, in Figs. 14–18 we have respectively plotted against $\ln K_n$ the values of ρ^*, p^*, N_1^*, Π^*, Q^*, and Q_θ^* at the inner boundary. The density, pressure, normal stress, and tangential heat flux show a singular behavior at $K_n = K_n^c$, while the shear stress and radial heat flux show, respectively, a steep inverted sigmoid and a sigmoid structure in the neighborhood of the critical Knudsen number. These figures suggest that the gas behaves qualitatively differently in the two regimes of K_n separated by the critical Knudsen number. In some respects these features remind us of a phase transition in thermodynamic systems. In order to see if there is any substance to this kind of imagination, we have calculated the entropy production at the inner boundary by using the results given in Figs. 14–18. The entropy production consists with the generalized hydrodynamic equations (2.18)–(2.21) taken for this work is given by the formula[2]

$$\sigma_{\text{ent}} = k_B g^{-1} \kappa \sinh\kappa \ , \tag{3.3}$$

where

$$g = (m_r/2k_B T)^{1/2}/(nd)^2 \ . \tag{3.4}$$

Thus we define a reduced entropy production by the expression

$$\hat{\sigma} = \kappa \sinh\kappa/\delta^2 \ , \tag{3.5}$$

since n is proportional to K_n^{-1}. The total reduced entropy production in the unit height of the volume between the two cylinders is then

$$\Sigma_{\text{total}} = 2\pi \int_{R_i}^{R_o} dr\, r\hat{\sigma}(r) \ .$$

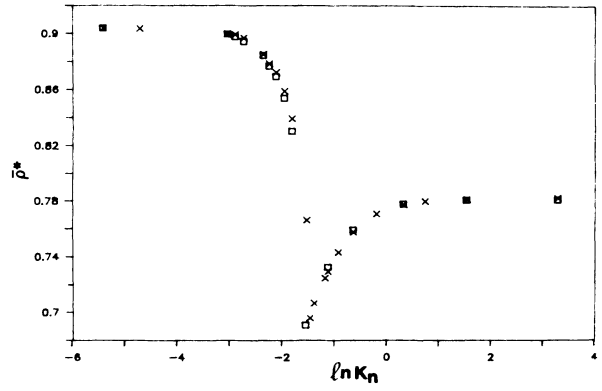

FIG. 14. Reduced density at the inner wall vs $\ln K_n$. $\times$, $q_c \neq 1$; $\square$, $q_c = 1$ (Maxwell–Cattaneo-Vernotte model).

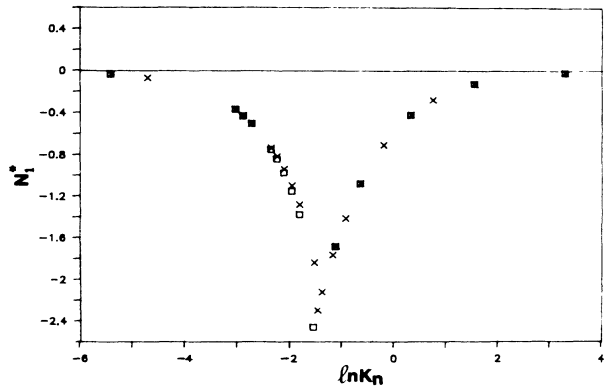

FIG. 16. Reduced normal-stress difference at the inner wall vs $\ln K_n$. The symbols have the same meaning as in Fig. 7.

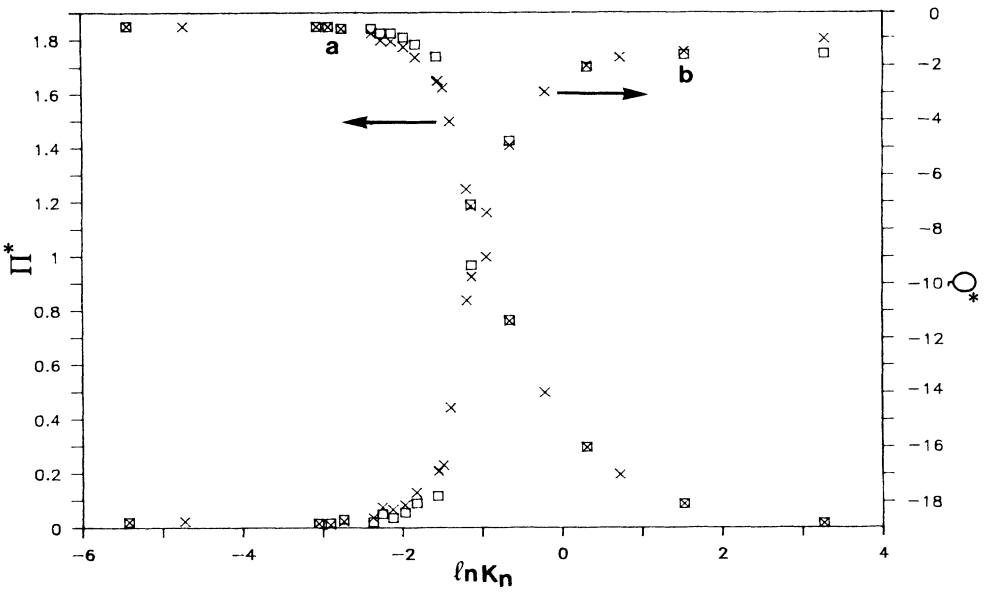

FIG. 17. Curve *a*, reduced shear stress at the inner wall vs $\ln K_n$. The symbols have the same meaning as in Fig. 7. Curve *b*, reduced radial heat flux at the inner wall vs $\ln K_n$. The symbols have the same meaning as in Fig. 7.

This can be calculated if the profiles are known for Π^*, N_1^*, Q^*, and Q_θ^* along with the temperature, pressure, and density. Since such calculations must be performed for many values of K_n in order to construct a $\Sigma_{\text{total}}-K_n$ curve and they are very time consuming to construct, we have simply calculated the entropy production at the inner boundary. Although only at $\xi=0$, this result conveys a very good idea of the global entropy production, since the profiles monotonically vanish as ξ increases to unity. In Fig. 19 is plotted against $\ln K_n$ the entropy production at the inner boundary. Interestingly, the entropy production shows a sharp singular behavior at $K_n=K_n^c$ and vanishes as K_n increases to infinity as it should, because the fluid becomes vacuous at $K_n=\infty$. The figure shows that the entropy production is continuous, but not analytic at the critical Knudsen number. Therefore the Knudsen number appears to be an order parameter that signifies the onset of a new "phase" of the fluid in which the fluid behavior is qualitatively different from that in the older "phase." In fact, judged from the figure, the fluid appears to undergo a "second-order phase transition" at $K_n=K_n^c$. We believe that this figure for $\hat{\sigma}$ provides a deeper understanding of the behavior exhibited by the fluid when the normal stresses are included in the generalized hydrodynamic equation. It says that the entropy production increases owing to the increasing normal stresses as δ or K_n increases, but the normal stresses cannot increase indefinitely since there is a hydrodynamic constraint imposed on it by (2.29) or (2.29′) and the system becomes vacuous. Then there is a point reached beyond which the normal stresses must diminish and consequently the entropy production, that is, an energy dissi-

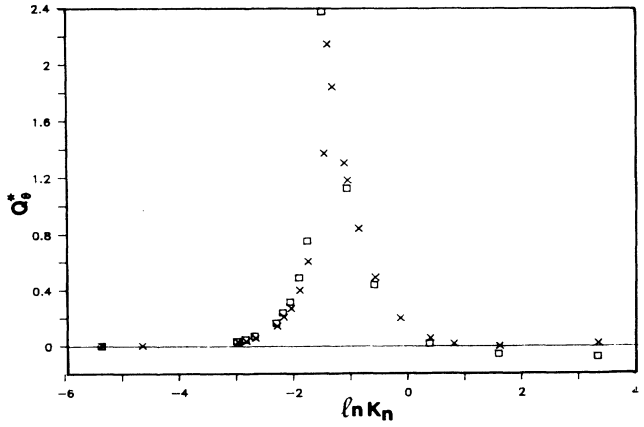

FIG. 18. Reduced tangential heat flux at the inner wall vs $\ln K_n$. The symbols have the same meaning as in Fig. 7.

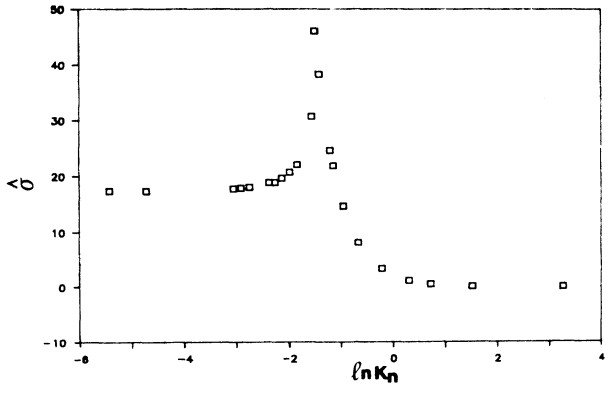

FIG. 19. Reduced entropy production at the inner wall vs $\ln K_n$. The reduced entropy production is logarithmic but continuous at K_n^c.

TABLE I. Fitting functions at the inner wall. $F=a+b\sinh^{-1}(12.5|K_n-K_n^c|)/|K_n-K_n^c|$ ($K_n^c=0.2257$).

F	a	b	Relative error (intercept)	Relative error (coefficient)
		Supercritical region		
ρ^*/K_n	−0.0835	0.2278	0.0631	0.0047
p^*/K_n	−0.0832	0.2286	0.0631	0.0047
N_1^*	0.0611	−0.1680	0.0463	0.0034
Π^*	−0.0432	0.1188	0.0328	0.0024
$(-Q^*)^{1/4}$	0.9678	0.0765	0.0219	0.0016
$Q_\theta^{*1/2}$	−0.0411	0.1082	0.0695	0.0052
η^*/K_n	−0.0960	0.1793	0.0687	0.0051
λ^*/K_n	−0.1264	0.2359	0.0904	0.0067
Δu	1.0167	−0.0740	0.0150	0.0011
		Subcritical region		
K_n/ρ^*	−0.4343	0.0558	0.0080	0.0017
K_n/p^*	−0.4298	0.0553	0.0076	0.0017
N_1^*	2.8608	−0.3704	0.0511	0.0111
K_n/Π^*	−0.2036	0.0263	0.0028	0.0006
K_n/Q^*	0.0199	−0.0026	0.0003	0.000 06
$Q_\theta^{*1/2}$	−1.6426	0.2186	0.0276	0.0060
K_n/η^*	−0.4845	0.0610	0.0171	0.0037
K_n/λ^*	−0.4119	0.0528	0.0082	0.0018
Δu	0	0	0	0

pation, must diminish and eventually vanish altogether. After all, a vacuum cannot dissipate energy. Neither is it able to support stresses. We remark that the reduced entropy production $\hat{\sigma}$ would be monotonically decreasing with K_n if the normal stresses were absent.

The K_n dependence of ρ^* p^*, N_1^*, Π^*, Q^*, and Q_θ^* shown in Figs. 14–18 can be summarized to a good approximation by the form

$$F=a+b\sinh^{-1}(12.5|K_n-K_n^c|)/|K_n-K_n^c| , \quad (3.6)$$

where a and b are constants and F stands for one of the quantities listed above or a function of the quantity in question. In Table I we list the values of a and b for the quantities along with the accuracy of fitting. Through these fittings and their quality we see that the singular behavior of the quantities shown in Figs. 14–18 is basically logarithmic. In view of the fact that the entropy production is given in terms of the quantities mentioned above, it is not difficult to see that it also has a logarithmic singularity. It is indeed the case as is evident from the following:

$$K_n^{1.7}/\hat{\sigma}=-0.004\,37+0.000\,551\sinh^{-1}(12.5|K_n-K_n^c|)/|K_n-K_n^c| \quad (3.7a)$$

for the subcritical region and

$$\hat{\sigma}=\{-0.2347+0.4766\sinh^{-1}[12.5(K_n-K_n^c)]/(K_n-K_n^c)\}^2 \quad (3.7b)$$

for the supercritical region. The standard deviations are, respectively, 8×10^{-5} and 0.2519 for the intercepts in (3.7a) and (3.7b) and 5×10^{-4} and 0.019, respectively, for the coefficients to the hyperbolic function. The fitting can be improved, but we believe a point is made about the K_n dependence of $\hat{\sigma}$.

In connection with the singular behavior shown above, it is also interesting to add the following. We have mentioned that the shear and normal stress are confined to the cone surface shown in Fig. 2. In fact, they follow a trajectory on the cone surface as the Knudsen number varies; see the dotted curve in Fig. 2. The trajectory is shown in Fig. 20, where the solid curves are equipressure (isobaric) contours on the cone surface which are projected on the (Π^*,N_1^*) plane at $p^*=0$. The squares represent the values of the set (Π^*,N_1^*) satisfying the generalized hydrodynamic equations (2.18)–(2.21) at the inner wall, i.e., their solution. The leftmost upper square (i) is for the highest value of p^* corresponding to the lowest K_n value. As K_n increases, the value of p^* decreases and the system moves toward the rightmost square (c) near $-2N_1^*/3=1.6$. When this point is reached, the discriminant Δ vanishes and the maximum point in $-(\frac{2}{3})N_1^*$ is reached. The system then must follow a path along which the magnitude of N_1^* decreases and the system moves toward the state of $p^*=0$ that is located at the origin of the three-dimensional space (Π^*,N_1^*,p^*). Thus the system follows the lower part of the trajectory and tends towards the origin as K_n increases. The abrupt turnaround of the trajectory in the three-dimensional space is intimately related to the singular phase-transition-like behavior in various macroscopic

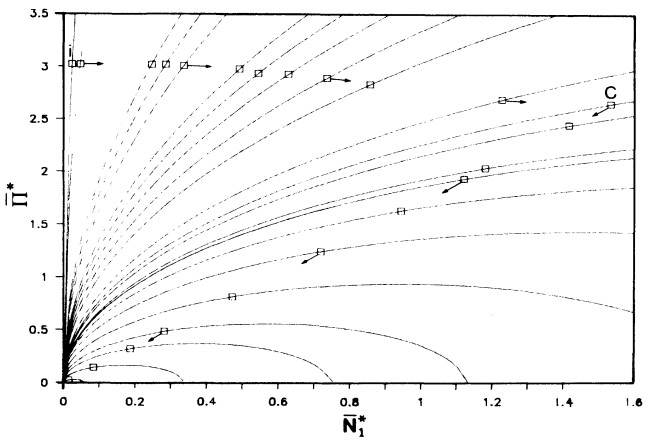

FIG. 20. Trajectory of shear-stress and normal-stress difference on the cone surface projected onto the $p^*=0$ plane. The solid curves are the equipressure ellipses defined by (2.29). The squares represent the solutions of the generalized hydrodynamic equations (2.18)–(2.21). As K_n increases, the solution tends toward the origin as indicated by the arrow. $\bar{\Pi}^*=(\frac{8}{3})^{1/2}\Pi^*$ and $\bar{N}_1^*=-(\frac{2}{3})N_1^*$.

properties as we have shown in Figs. 14–18, and point c is the state at which the discriminant vanishes for the first time. Note that the discriminant is equal to zero along the lower curve leading to the origin from point c. Such a singular behavior is due to the presence of N_1^*, which also forces the system to remain on the + half of the cone surface; see Fig. 2. Therefore the velocity slips we have seen arise from a combination of hydrodynamic and irreversible thermodynamic reasons as presented in this section. To these reasons will have to be added the surface–gas molecule scattering effects[21,22] in a more complete theory which takes into consideration the presence of boundaries in formulating generalized hydrodynamic equations. A formulation of such a theory is an open question at present.

The theoretical density profiles by either the present theory or the Monte Carlo direct simulation method show some noticeable deviations from the experimental data except at $K_n=0.0544$, although the deviations are invariably less than a few percent at most. Besides the experimental error, there is also an error inherent in the theoretical analysis which arises from the assumption that the length of the cylinders is infinite. This assumption is made to remove the end effects on the profiles and to simplify the theory, which otherwise would involve a larger set of generalized hydrodynamic equations since there would be a nonvanishing u_z component in the fluid velocity. It is not known at present how a nonvanishing u_z will affect the density profiles and other fluid properties. It will also be very helpful for developing a theory and ascertaining its validity if there are more detailed data especially in the boundary layers. We hope that the present work would induce such measurements in the future.

IV. DISCUSSION AND CONCLUDING REMARKS

In this work we have extended the previous calculations on flow profiles in cylindrical Couette flow of a Lennard-Jones fluid. The extension is achieved by including normal stresses in the generalized hydrodynamic equations. Normal stresses become significant in the intermediate range of Knudsen number in the neighborhood of the critical Knudsen number. In this intermediate range, owing to the inclusion of normal stresses, the dynamics of such a fluid is qualitatively changed from that which excludes the normal stresses. It is important to note that the Navier-Stokes theory in the present geometry is one example which neglects normal stresses and that the generalized hydrodynamic equations used in this work reduce in the Navier-Stokes and Fourier equations in the limit of $\delta\to 0$ or $K_n\to 0$.

Normal stresses put a constraint on the shear stress in the sense that normal and shear stresses must be confined to the stress-pressure cone surface (see Fig. 2), and this constraint and the fact that the vacuum cannot sustain stresses are the ultimate reason for the occurrence of a second-order phase-transition-like behavior of various fluid variables. The entropy production associated with this behavior is rather insightful; see Fig. 19. From this figure it is quite clear that the derivative of $\hat{\sigma}$ with respect to K_n will have a discontinuity, and this discontinuity is the reason for the terminology, second-order phase transition, that we have repeatedly used in connection with the singular behavior in fluid variables.

The density profiles that we have calculated and compared with experiment and the Monte Carlo direct simulation results are not too different from those in the previous work,[2] except for the appearance of thin boundary layers and a little flatter profiles in the high-Knudsen-number regime. It is important to point out that the high-K_n experimental data seem to exhibit a tendency for boundary layers near the walls although an incompleteness of the data would make this interpretation open to dispute. In any case, in the vicinity of the inner wall, the high-K_n results by the present theory are clearly inconsistent with the Monte Carlo direct simulation results.[5] The tendency for the gas molecules to accumulate near a rotating inner wall as predicted by the Monte Carlo method is against common intuition, although we have given a reason which we believe is behind the predicted phenomenon, on the basis of Nanbu's temperature and pressure profiles. If his prediction were indeed to be found consistent with the experimental fact, then the temperature and pressure profiles predicted by the Monte Carlo method would become more convincing.

The basic viewpoint taken in the present series of work[1,2,23] is that flow properties can be studied with stick boundary conditions, provided that nonlinear transport processes, in other words, generalized hydrodynamic equations, are used, instead of the Navier-Stokes and Fourier equations, for description of flow. This does not mean that surface–gas molecule interactions are unimportant for flow properties. We believe that there are two basic components influencing flow properties: one is surface–gas molecule interactions and the other is the bulk transport properties which can be generally nonlinear, especially when the parameter δ is not small. In this series of work *we have shown that nonlinear transport processes can be a major component to determine fluid*

flow properties and it is possible to describe them with the generalized hydrogeneralized hydrodynamic equations with stick boundary conditions. The generalized hydrodynamic equations can be further extended by following the procedure as described in the modified moment method.[3] We hope to report on a more complete theory that takes surface–gas molecule interactions more carefully into account than in the existing theories.[21]

Lastly, the following remark should be useful to the reader interested in transport processes in dense fluids. Although the generalized hydrodynamic equations are applied to a rarefied gas in the present series of work,[1,2] they can be applied to fluid dynamics of dense fluids if appropriate linear transport coefficients (i.e., η_0 and λ_0) are supplied as functions of density and temperature. In fact, since the expressions for η_0 and λ_0 used in the present work are believed to be valid up to the triple point density of argon, one can calculate its nonlinear flow properties up to the triple point by using (2.18)–(2.21). This hydrodynamic method would thereby provide, for example, effective transport coefficients which can be compared with those obtained by means of nonequilibrium molecular dynamics methods or Monte Carlo simulation methods. This line[18,20] of study has been pursued in a semiempirical manner in the past since linear transport coefficients are taken as adjustable parameters, but it would be worthwhile to compute them numerically and then combine the results with the generalized hydrodynamic equations in order to calculate nonlinear fluid properties. This line of study is actively pursued at present and will be reported in the future.

Note added in proof. Equation (2.12d) in Ref. 2 is in error. There should be added $-2p\beta$ on the right-hand side of the equation. The last term in (2.6) in Ref. 2 should read $-p(\rho\hat{\Delta}+p)\sinh\kappa/\kappa\eta_{b0}$. The additional pressure term is unfortunately missing in all the previous papers of this series. We would like to correct the error on this occasion. The results of Ref. 2 are not affected by these errors.

ACKNOWLEDGMENT

This work has been supported in part by the National Sciences and Engineering Research Council of Canada, which is gratefully acknowledged for its support.

*Also at the Physics Department, McGill University, Montreal, Quebec, H3A 2T8, Canada.

[1]D. K. Bhattacharya and E. C. Eu, Phys. Rev. A **35**, 821 (1987).

[2]R. E. Khayat and B. C. Eu, Phys. Rev. A **38**, 2492 (1988).

[3]B. C. Eu, J. Chem. Phys. **73**, 2958 (1980); **74**, 2998 (1981); **74**, 3006 (1981); **80**, 2123 (1984); **82**, 4283 (1985); **74**, 6362 (1981); **87**, 1220 (1987).

[4]B. C. Eu, Ann. Phys. (N.Y.) **140**, 341 (1982); J. Nonequil. Thermodyn. **11**, 211 (1986); Acc. Chem. Res. **19**, 153 (1986).

[5]K. Nambu, Phys. Fluids **27**, 2632 (1984).

[6]D. J. Alofs and G. S. Springer, Phys. Fluids **14**, 298 (1971).

[7]M. N. Kogan, *Rarefied Gas Dynamics* (Plenum, New York, 1969).

[8]G. Jaumann, Sitzungsber. Akad. Wiss. Wien. Math. Naturwiss. Kl. Abt. 2A **120**, 385 (1911); W. Prager, *Introduction to Mechanics of Continua* (Ginn, Boston, 1961).

[9]B. C. Eu, J. Chem. Phys. **82**, 3773 (1985).

[10]B. C. Eu, R. E. Khayat, G. D. Billing, and C. Nyeland, Can. J. Phys. **65**, 1090 (1987).

[11]T. C. Lin and R. E. Street, National Advisory Committee for Aeronautics Report No. 1175, 1954 (unpublished).

[12]S. Chapman and T. G. Cowling, 3rd ed. *Mathematical Theory of Non-Uniform Gases* (Cambridge University Press, London, 1970).

[13](a) W. T. Ashurst and W. G. Hoover, Phys. Rev. A **11**, 658 (1975); (b) B. C. Eu, Ann. Phys. (N.Y.) **120**, 423 (1979).

[14](a) M. Reiner, in *Proceedings of the Fourth International Congress on Rheology, Providence, 1963,* edited by E. H. Lee (Interscience, New York, 1965), p. 267; (b) C. Truesdell and W. Noll, in *The Nonlinear Field Theories of Mechanics,* Vol. 3 of *Handbuch der Physik,* edited by S. Flügge (Springer, Berlin, 1965), Teil. 3.

[15]G. A. Bird, *Molecular Gas Dynamics* (Oxford University Press, London, 1976).

[16]J. C. Maxwell, Philos. Trans. R. Soc. London, Ser. A **157**, 49 (1867).

[17]C. Cattaneo, C. R. Acad. Sci. **247**, 431 (1958); P. Vernotte, *ibid.* **247**, 3154 (1958).

[18]B. C. Eu, J. Chem. Phys. **79**, 2315 (1983); Phys. Lett. **96A**, 29 (1983); Y. G. Ohr and B. C. Eu, *ibid.* **101A**, 338 (1984); J. Chem. Phys. **81**, 2756 (1984); B. C. Eu, *ibid.* **82**, 4683 (1985); D. K. Bhattacharya and B. C. Eu, Phys. Rev. A **35**, 4850 (1987).

[19]K. Walters, *Rheometry* (Chapman and Hall, London, 1975), Chap. 4.

[20]B. C. Eu (unpublished).

[21]H. Grad, Commun. Pure Appl. Math. **2**, 331 (1949); P. Welander, Ark. Fys. **7**, 507 (1954); E. P. Gross, E. A. Jackson, and S. Ziering, Ann. Phys. (N.Y.) **1**, 141 (1957); J. R. Dorfman and H. van Beijren, in *Statistical Mechanics,* edited by J. J. Berne (Plenum, New York, 1977), Part B, pp. 65–179.

[22]See, for example, F. O. Goodman and H. Y. Wachman, *Dynamics of Gas Surface Scattering* (Academic, New York, 1976).

[23]B. C. Eu, Phys. Rev. A **36**, 400 (1987).